

# Van der Waals interlayer potential of graphitic structures: from Lennard-Jones to Kolmogorov-Crespy and Lebedeva models.

Zbigniew Koziol\*,<sup>1</sup> Grzegorz Gawlik,<sup>2</sup> and Jacek Jagielski<sup>1,2</sup>

<sup>1</sup>*National Center for Nuclear Research, Materials Research Laboratory,  
ul. Andrzeja Sołtana 7, 05-400 Otwock-Świerk, Poland*

<sup>2</sup>*Institute of Electronic Materials Technology, 133 Wólczyńska Str., 01-919 Warszawa, Poland*

The experimental knowledge on interlayer potential of graphenites is summarized and compared with computational results based on phenomenological models. Besides Lennard-Jones approximation, the Mie potential is discussed, Kolmogorov-Crespy model and equation of Lebedeva et al. An agreement is found between a set of reported physical properties of graphite (compressibility along *c*-axis under broad pressure range, Raman frequencies for bulk shear and breathing modes under pressure, layer binding energies), when a proper choice of model parameters is made. It is argued that the Kolmogorov-Crespy potential is the preferable one for modelling. A simple method of fast numerical modelling, convenient for accurate estimation of all these discussed physical properties is proposed. It is useful in studies of other van der Waals homo/heterostructures.

PACS numbers: 61.46.-w, 73.20.At, 73.22.-f 61.48.De, 68.35.Gy, 73.22.Pr

## INTRODUCTION.

There is recently a growing interest in artificial heterostructures formed by 2-dimensional layers of graphene and other newly discovered materials, like these of transition metal dichalcogenides (TMDCs), and named 'van der Waals heterostructures' [1]. The reason of that is reachness of physical phenomena observed and high potential of their possible applications [2]. Moiré patterns result when two layers are rotated [3], [4] and are related to van Hove singularities. Recently, in bilayer graphene twisted at 1.1 degree superconductivity was found with critical temperature of 1.7K [5]. By manipulating doping levels these singularities are observed at angles up to 31 degrees [6]. It was shown that free-standing vdW heterostructure of graphene on hexagonal boron nitride (hBN), where a small lattice mismatch exists shows a buckled atomic structure formed as Moiré pattern [7]. There is already a number of laboratory prototypes of optoelectronic devices [8], like bolometers [9], photodetectors [10], [11]. Their characteristics can be tuned by elemental doping, surface chemical doping, intercalation and electrostatic gating.

It is believed that artificial van der Waals heterostructures offer a broad field for research on novel materials for graphene/silicene, graphene/*MoS*<sub>2</sub>, and silicene/*MoS*<sub>2</sub> systems [2], as well silicene [12] or *MoS*<sub>2</sub> alone [13]. Ab-initio calculations suggest the existence of magnetism in *ReS*<sub>2</sub> doped with Co, Fe, and Ni [14]. Formation of quantum-well Type-I heterostructure in van der Waals - interacting monolayers of *MoS*<sub>2</sub> and *ReS*<sub>2</sub> has been demonstrated [15] and Type-II band alignment was found in vdW heterojunction diodes based on *InSe* and *GaS*

and graphene [16]. *WSe*<sub>2</sub> and *MoS*<sub>2</sub> monolayers have been shown useful to create charge density modulation in electronic band valleys, resulting in valley polarization, and *Na*-doped *WS*<sub>2</sub> under strain is considered a candidate for spintronics [17]. After spin injection from a ferromagnetic electrode transport of spin-polarized holes within the *WSe*<sub>2</sub> layer was observed [18]. hBN and graphene vdW heterojunctions indicate on large potential of their use in spintronics [19]. Light-induced negative differential transconductance phenomenon was realized on graphene/*WSe*<sub>2</sub> heterojunction transistor [20]. DFT calculations show that vdW interactions dominate between antimonene and graphene layers and by applying electric field between them one can tune the height and type of Schottky contacts [21]. Lattice dynamical theory and ab initio calculations indicate on the existence of piezoelectricity in 2D lattices comprising h-BN, *2H* - *MoS*<sub>2</sub>, and other transition-metal dichalcogenides [22].

It is generally thought that van der Waals interaction, ubiquitous in nature, is caused by temporal fluctuations of electronic charge that induces dipoles of random amplitude [23]. It plays a role in friction and adhesion between materials, absorption of molecules on surfaces. These relatively weak forces are responsive for binding between separate sheets of graphene.

While many electronic properties of graphene-based systems are known [24] still there are open questions concerning the detailed form and physical mechanisms leading to inter-plane potential in these systems. There are two types of approaches used to describe the van der Waals potentials of graphitic systems: an ab-initio one, based on density functional theory, and the other uses empirical potentials [25].

The DFT calculations often give an underestimated values of binding energy energy in case of van der Waals interactions [26], [27], [28], [29], [30] and energy differ-

---

\*e-mail: zbigniew.koziol@ncbj.gov.pl

ence between bindings of (preferred) AB and AA type of stacking,  $E_{AB}$  and  $E_{AA}$ , which seems too large, as we will discuss. Recent diffusion quantum Monte Carlo calculations predict for instance  $E_{AA}/E_{AB}$  of about 0.65 [31]. Results however depend strongly on the functionals used to model vdW forces [32], [33].

In this work we compare how well several properties of graphene/graphite can be described by using a few empirical potentials. Some of them are well based on DFT calculations. An advantage of using empirical potentials relies on ease of their implementation in any numerical methods. Moreover, we describe a scheme of computing several basic properties based on a simple analytical approach. The method may be easily extended to investigation of vdW homo- and heterostructures other than graphene/graphite. We demonstrate that by careful choosing of parameters of phenomenological potentials we may reproduce self-consistently experimental values of compressibility of graphite as well Raman shifts observed in shear mode under pressure and predict change of Raman shift under pressure for layer breathing mode (LBM).

### Lennard-Jones and Mie Potentials.

An often used approximation of vdW potential is the 12-6 Lennard-Jones one,  $U(r) = 4\epsilon((\sigma/r)^{12} - (\sigma/r)^6)$ , with two only adjustable parameters, where  $r$  is distance between atoms.

It reproduces well interlayer distance and elastic constant of graphite. It was proved useful in describing several basic properties of  $C_{60}$  molecules [34], with  $\epsilon = 2.964\text{meV}$ ,  $\sigma = 3.407\text{\AA}$ . It was used for modeling carbon nanotubes [35], with  $\epsilon = 4.656\text{meV}$  and  $\sigma = 3.825\text{\AA}$ . He et al. [36] obtain an analytical approximation for vdW

forces acting between nanotubes. Authors extend their continuum model [37] to study vibrations of multilayered graphene sheets. It is a convenient approximation in modeling reinforcement of composite materials with carbon nanotubes [38].

A more general form of vdW potential is one introduced by Mie [39], [40] and it often reproduces well properties of carbon compounds,  $U(r) = \alpha\epsilon((\sigma/r)^m - (\sigma/r)^n)$ , where  $\alpha = (m/(m-n)) \cdot (m/n)^{n/(m-n)}$ . When  $m = 12$  and  $n = 6$ , the form of Lennard-Jones potential, with  $\alpha = 4$  is assumed.

### Kolmogorov-Crespi and Lebedeva Potentials.

There are at least two deficiencies of LJ or Mie type of potentials. First is that they are isotropic, i.e. the potential depends on distance between atoms, only. However, in graphenites, the binding between atoms on different planes is due to overlap between  $\pi$  electrons from adjacent layers and as such it ought to depend on the angle between orbitals. The second problem, as it was noticed first by Kolmogorov and Crespi [41], [42] and will also be shown in this work, is that these potentials produce too small energy difference between bindings of (preferred) AB and AA type of stacking,  $E_{AB}$  and  $E_{AA}$ . Albeit there is some controversy about how large that energy difference is. The KC potential has an  $r^{-6}$  two-body van der Waals-like attraction and an exponentially decaying repulsion terms, very short ranged, falling essentially to zero at two transverse interatomic distances. The directionality of the overlap is reflected by a function which rapidly decays with the transverse distance  $\rho$  (Fig. 1). Most often it is used in the following form, for interaction between atoms  $m$  and  $l$ :

$$U_{lm} = -A \left( \frac{z_0}{r_{lm}} \right)^6 + \exp(-\lambda(r_{lm} - z_0)) \cdot [C + f(\rho_{lm}) + f(\rho_{ml})] \quad (1)$$

$$\rho_{lm}^2 = r_{lm}^2 - (\mathbf{n}_l \mathbf{r}_{lm})^2 \quad (2)$$

$$\rho_{ml}^2 = r_{lm}^2 - (\mathbf{n}_m \mathbf{r}_{lm})^2 \quad (3)$$

$$f(\rho_{lm}) = \exp(-(\rho_{lm}/\delta)^2) \cdot \sum_{n=0}^2 C_{2n} (\rho_{lm}/\delta)^{2n} \quad (4)$$

where  $\mathbf{n}_k$  is the vector normal to the  $sp^2$  plane in the vicinity of the atom  $k$ , and  $z_0$  is close to the interlayer distance at equilibrium. The summation over  $n$  in Eq. 4 is usually limited from  $n = 0$  to  $n = 2$  [43].

KC potential has been used broadly in numerical mod-

eling (molecular dynamics) [3], [4], [44],[45] as well in description of ballistic nanofriction [46], [47].

Lebedeva et al. [48], [49] use another form of anisotropic potential which was obtained by fitting DFT calculations and was found to describe well the ex-

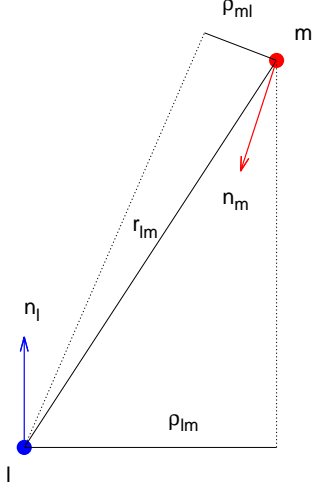


FIG. 1: Schematics of Kolmogorov-Crespi interaction between atoms I and  $m$  located on different flakes of graphene. The vector  $\mathbf{n}_k$  ( $k=1,m$ ) is normal to the  $sp^2$  plane in the vicinity of atom  $k$ .

perimental graphite compressibility and the corrugation against sliding, while Jiang [50] uses 5 for modeling thermal conductivity of FLG:

$$U = -A \left( \frac{z_0}{r} \right)^6 + B \exp(-\alpha(r - z_0)) + C (1 + D_1 \rho^2 + D_2 \rho^4) \exp(-\lambda_1 \rho^2) \exp(-\lambda_2 (z^2 - z_0^2)) \quad (5)$$

where  $r$  is the interatomic distance and  $\rho = \sqrt{r^2 - z^2}$  is the projection of the distance within the graphene plane.

### ANALYTICAL APPROXIMATION.

Lattice spacing in graphene in hexagonal  $c$ -direction, is known well from X-ray diffraction, it is  $3.3538 \text{ \AA}$  at room temperature, and it does not change strongly with temperature [51]. The equilibrium interlayers spacing is  $3.34 \text{ \AA}$  in AB stacked [51] and  $3.44 \text{ \AA}$  in turbostratic graphene [52]. Neutron diffraction studies show that all in-plane C-C lengths are  $1.422 \text{ \AA} \pm 0.001 \text{ \AA}$  ([53]).

#### Distances between atoms in AB and AA stacking.

There are two types of ordering of atoms on the nearest plane with respect to atoms on another plane. Let us call

them type I and type II ordering. The type I results when atom is placed over another atom of the hexagon and type II when atom is placed over the center of hexagon. Type I ordering is the only one in case of AA stacking, and in case of AB stacking equal number of atoms is in ordering of type I and II.

We can create a convenient scheme of calculating numerically potential energy for different stackings by computing it for each of these types of orderings. For that, we need distances projection (in plane) between an atom position over the plane together with number of atoms at these distances (rings of equi-distant atoms, as these in Fig. 2). These numbers can be found quickly with custom written scripts that compute distance between atoms in a graphene structure which was build also by scripts. The results are provided in Tables I and II, for both types of ordering. Analytical expressions on these distances are available however we do not know a method to express by formula the number of atoms in equi-distant rings.

In numerical simulations, e.g. performed in LAMMPS [43], it is a standard procedure to introduce a cut-off distance in Equations ?? – 5. Potential energy between particles exceeding that distance is assumed to be equal zero, while the function given by these equations is appropriately smoothed out at that distance in order to avoid possible discontinuities in computational results. That cut-off is taken usually at around  $12 \text{ \AA}$  in case of graphene modelling.

Limiting any approximation to atoms listed in Tables I and II is equivalent of using cut-off distance in Eq. ?? of about  $15.4 \text{ \AA}$  and then we expect to obtain the same accuracy of results as by using LAMMPS.

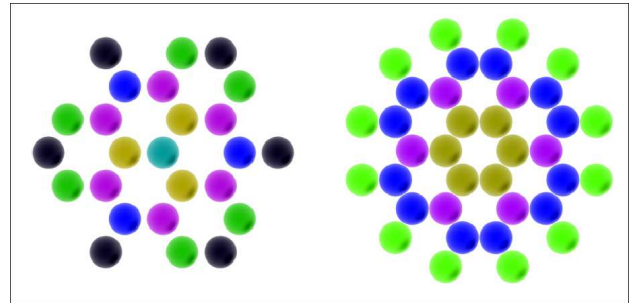


FIG. 2: Rings of equi-distant atoms on neighbouring planes of graphene. On the left is type I, present for AA and AB stacking and type II (right) present in AB stacking, only.

TABLE I: Distance between an atom on one graphene plane and nearest neighbors on next plane, for type I of neighbors, as in Fig. 2 (left), found in AA and AB stacking of layers.  $\mathbf{N}$  is number of neighbors and  $\mathbf{d}$  is distance (in units of graphene unit cell value of 1.42 Å).

$\mathbf{d}$	0	1	1.7321	2	2.6458	3	3.4641	3.6056	4	4.3589	4.5826	5	5.1962	5.2915
$\mathbf{N}$	1	3	6	3	6	6	6	6	3	6	12	3	6	6
$\mathbf{d}$	5.5678	6	6.0828	6.245	6.5574	6.9282	7	7.2111	7.5498	7.8102	7.9373	8	8.1854	8.544
$\mathbf{N}$	6	6	6	12	6	6	9	6	12	6	12	3	6	6
$\mathbf{d}$	8.6603	8.7178	8.8882	9	9.1652	9.5394	9.6437	9.8489	10	10.1489	10.3923	10.4403	10.5357	
$\mathbf{N}$	6	6	6	6	12	12	12	6	3	6	6	6	12	

TABLE II: Distance between an atom on one graphene plane and nearest neighbors on next plane, for type II of neighbors, as in Fig. 2 (right), found in AB stacking of layers.  $\mathbf{N}$  is number of neighbors and  $\mathbf{d}$  is distance (in units of graphene unit cell value of 1.42 Å).

$\mathbf{d}$	1	2	2.6458	3.6056	4	4.3589	5	5.2915	5.5678	6.0828	6.5574	7	7.2111
$\mathbf{N}$	6	6	12	12	6	12	6	12	12	12	12	18	12
$\mathbf{d}$	7.8102	8	8.1854	8.544	8.7178	8.8882	9.5394	9.8489	10	10.1489	10.4403	10.583	
$\mathbf{N}$	12	6	12	12	12	12	24	12	6	12	12	12	

Potential energy  $\Phi_I(z)$  for an atom in position AA at a distance  $z$  from the plane will be given by an infinite sum of contributions from equi-distant atoms of type  $I$ :

$$\Phi_I(z) = \sum_{i=1}^{\infty} N(i) \cdot U \left( \sqrt{z^2 + (a \cdot d_i)^2} \right), \quad (6)$$

where the number of neighbors  $N(i)$  at distance  $d(i)$  is taken from entries of Table I and  $U$  is any of potentials discussed (LJ, Mie, KC or Lebedeva's). In Eq. 6,  $a$  is the unit cell length for in-plane atoms ( $a = 1.42$  Å in case of graphene).

In case of AB planes, there is equal number of atoms that are in ordering of type  $I$  and type  $II$ . Equation on energy for type  $II$  atoms,  $\Phi_{II}(z)$ , is similar as 6, with summation taken on the data in Table II. We must take

an average of  $\Phi_I(z)$  and  $\Phi_{II}(z)$  as an average energy of each atom in case of AB ordering.

Figure 3 illustrates quick convergence of potential energy  $\Phi$  as a function of the total number of atoms  $N$  in a symmetric "molecule" for type I and type II "molecules" computed for LJ potential. An approximately  $1/N^2$  scaling, when the rings of equi-distant neighbours are added in Eq. 6.

Hence, an average potential energy for an atom at distance  $z$  from the surface of bulk graphite is given as a sum, for AA, AB, and ABC stackings, respectively:

$$E_{AA}(z) = \sum_{i=1}^{\infty} \Phi_I(z + ic). \quad (7)$$

$$E_{AB}(z) = \sum_{i=1}^{\infty} \frac{1}{2} (\Phi_I(z + (2i - 1)c) + \Phi_{II}(z + (2i - 1)c)) + \sum_{i=1}^{\infty} \Phi_I(z + 2ic), \quad (8)$$

$$\begin{aligned} E_{ABC}(z) = & \frac{1}{2} \sum_{i=1}^{\infty} [\Phi_I(z + 3ic) + \Phi_{II}(z + 3ic)] \\ & + [\Phi_I(z + (3i - 1)c) + \Phi_{II}(z + (3i - 1)c)] \\ & + [\Phi_I(z + (3i - 2)c) + \Phi_{II}(z + (3i - 2)c)]. \end{aligned} \quad (9)$$

In our numerical computation we limit the number of planes in Eqs 7–9 to 4, since contribution to potential

energy from next planes diminishes quickly: it is of the order of 90%, 10%, 2% and 0.5% for the first, second,

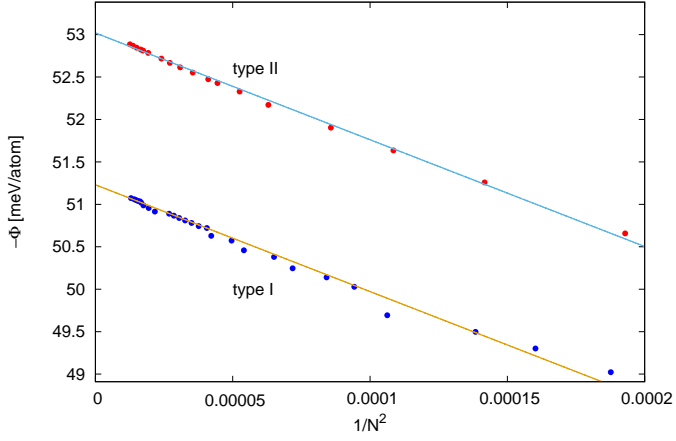


FIG. 3: Scaling of potential energy depth as a function of  $1/N^2$ , the number of atoms in a symmetric "molecule" for type I and II molecules, computed for LJ potential with parameters  $\epsilon = 2.80 \text{ meV}$  and  $\sigma = 3.38 \text{ \AA}$ . Asymptotic splitting for  $N \rightarrow \infty$  between type I and type II energy minima,  $(\Phi_{II} - \Phi_I)/\Phi_{II}$ , is 0.034. Potential of type I is related to potential in AA stacking, while potential in AB stacking is an average of potentials of type I and II.

third and fourth plane, respectively (Fig. 4). Considering 4 planes only is equivalent to assuming cut-off distance of  $5c$ , that is  $16.7 \text{ \AA}$ .

The proposed method of computing interlayer potential is convenient for quick testing of potentials other than that of Mie or Lennard-Jones as well, since that requires only replacement of the function  $U(z)$  in Eq. 6 by another one.

In case of perfect AA or AB stacking, due to symmetry,  $\pi$ -orbitals must point out in directions normal to planes. In that case, in Kolmogorov-Crespi Equations 4, values of  $\mathbf{n}_l \mathbf{r}$  and  $\mathbf{n}_m \mathbf{r}$  reduce to  $z$ , where  $z$  is distance of an atom from the plane. That is,  $\rho_{lm}$  and  $\rho_{ml}$  become equal to  $d$  from Tables I and II. We may rewrite Equations 4 in this form:

$$U_{KC}(x) = -A \left( \frac{z_0}{r} \right)^6 + \exp(-\lambda(r - z_0)) \cdot \left[ C + 2 \exp(-(d/\delta)^2) \cdot \sum_{n=0}^2 C_{2n} (d/\delta)^{2n} \right], \quad (10)$$

Similarly, we may rewrite Lebedeva's version of potential:

$$U_{Leb}(x) = -A \left( \frac{z_0}{r} \right)^6 + B \exp(-\alpha(r - z_0)) + C (1 + D_1 d^2 + D_2 d^4) \exp(-\lambda_1 d^2) \exp(-\lambda_2 (z^2 - z_0^2)). \quad (11)$$

In 10 and 11,  $r = \sqrt{z^2 + d^2}$ .

TABLE III: Summary of parameters' values used in Kolmogorov-Crespi equation 10.

A [meV]	C [meV]	$C_0$ [meV]	$C_2$ [meV]	$C_4$ [meV]	$z_0$ [Å]	$\lambda$ [Å <sup>-1</sup> ]	$\delta$ [Å]	Ref.
10.238	3.030	15.71	12.29	4.933	3.34	3.629	0.578	[42],[47]
9.89	0.7	5.255	2.336	1.168	3.449	3.2	2.1	this work, set A
8.881	0.6286	4.719	2.098	1.049	3.487	3.4	1.7	this work, set B

TABLE IV: Summary of parameters' values used in Lebedeva equation 11.

A [meV]	B [meV]	C [meV]	$\alpha$ [Å <sup>-1</sup> ]	$z_0$ [Å]	$\lambda_1$ [Å <sup>-2</sup> ]	$\lambda_2$ [Å <sup>-2</sup> ]	$D_1$ [Å <sup>-2</sup> ]	$D_2$ [Å <sup>-4</sup> ]	Ref.
10.510	11.652	35.883	4.16	3.34	0.48703	0.46445	-0.86232	0.10049	[48]
14.558	21.204	1.8	4.16	3.198	0.6	0.4	-0.862	0.10049	this work

In case of Lennard-Jones potential, results presented here are computed with  $\epsilon = 2.4 \text{ meV}$  and  $\sigma = 3.4322$ .

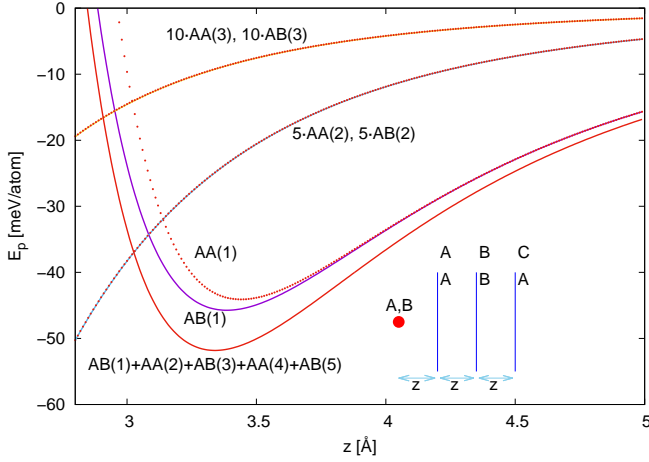


FIG. 4: Contribution to potential energy of a single atom (represented by large red dot in the insert) as a function of distance  $z$  from the surface of three neighbouring planes, separated also by distance  $z$ . The case of ABA and ABC ordering of planes is considered. The atom is considered in two positions with respect to the first plane, AA(1) or AB(1). The energy contribution from the third plane is exactly the same regardless whether it is A plane or C plane. Energy from the second and third planes are rescaled 5 and 10 times, respectively. Classical L-J potential 12-6 with parameters  $\epsilon = 2.80 \text{ meV}$  and  $\sigma = 3.38 \text{ \AA}$  was used. The depth of potential well for the lowest curve denoted as "AB(1)+AA(2)+AB(3)+AA(4)+AB(5)" (which shows the sum of energies from 5 consecutive planes in AB configuration) is 52 meV.

For models of Kolmogorov-Crespi and Lebedeva et al. we used values of parameters as listed in tables III and IV, respectively[77]. One ought to be aware that usually there is a broad range of parameters values for any of the above models of potential that may provide a functionally nearly identical dependencies  $U(z)$  and reasonable agreement with experiments; compare for instance [42],[47] with [41] and [45]. The original parameters of Lebedeva equation were derived by fitting to results of *ab-initio* DFT modeling and with the purpose of describing graphene corrugation experiments. While we recognize the usefulness of proposed new equations for providing phenomenological description of certain materials properties, we find no strong justification for adhering to original values of parameters. In particular, as we discuss later, the value of  $C$  in Table IV proposed in the original work is likely significantly too large.

The meaning of some parameters is as follows.  $\sigma$  and  $z_0$  decide most about position of potential minimum (equilibrium interlayer spacing), which is also sensitive to  $D_2$  and  $\lambda_2$ , while  $\lambda$ ,  $\delta$ ,  $\lambda_1$  and mainly  $C$  in Eq. 11 decide most about AB-AA energy difference at potentials minima. Value of  $\lambda$  influences mostly the slope of  $dE/dz$  in Fig. 4 on low- $z$  side of potential curve and as a consequence it decides about the compressibility as a function

of pressure.

### Compressibility.

Equation 8 may be used for computing compressibility along  $c$ -axis, since force and pressure acting on a particle is proportional to derivative of potential energy:

$$P(c) = \eta \cdot \frac{dE_{AB}(c)}{dc}, \quad (12)$$

where  $c$  is lattice constant perpendicular to the planes under pressure  $P$  and  $\eta$  is the number of atoms per unit area,  $\eta = 61.171 \text{ GPa} \cdot \text{eV}^{-1} \cdot \text{\AA}^{-3}$  for graphene. The first (Eq. 12) and second derivatives of  $E_{AB}(z)$  could be computed by using derived analytical expressions. Numerical approach of finding derivatives is however convenient to implement and fast.

Figure 5 shows the found ratio of  $c/c_0$  as a function of pressure for LJ, KC and Lebedeva potentials, with parameters as these in Tables III and IV. In case of LJ model, the parameter  $\epsilon$  used was  $3.3 \text{ meV}$ , which leads to binding energy of  $64 \text{ meV/atom}$ , larger than most commonly accepted value of around  $50 \text{ meV/atom}$  but leading to better agreement between results of other calculations and measurements, as reported in the following sections. The straight solid line with a slope of  $-0.029/\text{GPa}$  at  $P = 0$  for LJ potential corresponds to elasticity modulus  $C_{33} = 38.5 \text{ GPa}$ , and for KC one the slope gives  $C_{33} = 43.5 \text{ GPa}$ , in a very good agreement with experiment. *Ab-initio* DFT computations result in a broader spread of values, from 43.6 to 67.5 GPa [54].

Pressure dependence of  $c$  can be found or deduced from several measurements ([55], [56], [57], [58], [53]). Experimental results in Fig. 5 have a broad dispersion of data points, which is, in part, due to subtle differences in the used measurement techniques.

### Stacking order

There is much controversy around prevailing stacking order in graphite and in a few layers graphene (FLG).

It is known that there are three types of stacking, an AA one, which is simple hexagonal (it is not found in natural graphite and exists only in intercalated compounds such as  $C_6Li$  and  $C_8K$ , an AB stacking, hexagonal, known also as Bernal, and a rhombohedral ABC stacking. Additionally, a random stacking of these three types is called a turbostratic TS structure and often is obtained in laboratories. In bulk graphite, it was reported that the volume fraction AB:ABC:TS was about 80:14:6 ([60]).

Lee et al. [61] were able to obtain AA structured graphene on diamond surface, with an interplanar spac-

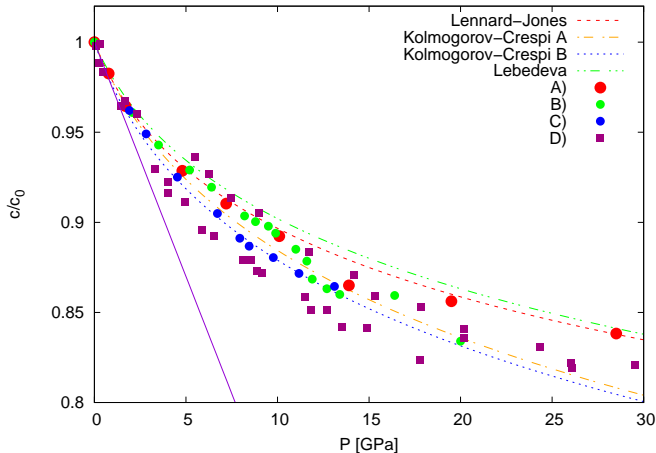


FIG. 5: Compressibility of graphite along c-axis. The solid curves are computed numerically by using Eq. 12 with L-J, K-C, and Lebedeva potentials. Datapoints are collected from works of Lynch and Drickamer ([56], A), Zhao and Spain ([57], B), Hanfland et al. ([59], C), Clark et al. ([58], D).

ing of  $\sim 3.55\text{\AA}$ . That value is between that of the AB graphite ( $3.35\text{\AA}$ ) and the Lithium intercalated AA graphite  $3.706\text{\AA}$  [62]. Norimatsu and Kusunoki [63] observe ABC-stacked graphene on the *SiC* substrate and

interpret their results in terms of possible modification of second-plane interactions by the substrate, as explained by Slonczewski-Weiss-McClure model [64]. Yoshizawa et al. [65] propose that the AB stacking of layers in graphite is a consequence of orbital interactions between layers rather than of generally accepted van der Waals forces.

The energy difference between AA and AB is reported, to be  $17.31\text{ meV/atom}$  ([31]), in favour of AB, while between ABC and AB it was reported as  $0.11\text{ meV/atom}$  ([66]), which are both based however on DFT calculations, only.

It was observed that in the case of graphene, its bilayer exhibits AB stacking while trilayer prefers ABC stacking [67]. When the number of layers increases, again AB stacking is favored. The binding energies are found to increase from  $23\text{ meV/atom}$  in bilayer to  $39\text{ meV/atom}$  in pentalayer, while the interlayer distance decreases from  $3.37\text{\AA}$  in bilayer to  $3.35\text{\AA}$  in pentalayer. Our models do not reproduce so strong change of binding energy with number of layers. In 2-layer graphene we find around 90% of binding energy per atom of that in bulk graphite, when LJ model is used (Fig. 4). However, the change of interlayer distance agrees with that reported [68], for all three models discussed.

TABLE V: Energies of FLG with number of layers from 2 to 6, for AA, AB and ABC stacking.

ordering	2 layers	3 layers	4 layers	5 layers	6 layers
AA	AA(1)	2AA(1)+AA(2)	3AA(1)+2AA(2)+AA(3)	4AA(1)+3AA(2)+2AA(3)	5AA(1)+3AA(2)+3AA(3)+2AA(4)
AB	AB(1)	2AB(1)+AA(2)	3AB(1)+2AA(2)+AB(3)	4AB(1)+3AA(2)+2AB(3)	5AB(1)+4AA(2)+3AB(3)+2AA(4)
ABC	-	2AB(1)+AA(2)	3AB(1)+2AB(2)+AA(3)	4AB(1)+3AB(2)+2AA(3)	5AB(1)+4AB(2)+3AA(3)+2AB(4)

If to assume that interaction between next nearest planes (NNP) is negligible than there is no reason for difference in stability of ABC and AB structures. Hence (NNP) interaction must play a role. Table V summarizes total potential energy of a FLG. The notation used there is the same as in Fig. 4, and it should be understood as follows (taking AB stacking for 3 layers, as an example):  $2AB(1)+AA(2)$  means that we have 2 pairs of layers in AB stacking that are apart for  $1c$ , and one pair of AA ordering of layers apart for  $2c$ . One should notice that energy of AC stacking is the same as that of AB, since atoms configuration of neighboring planes are the same in both cases. We see from Table V that for 4 and more layers ABC stacking is energetically favorable. However the energy difference between AB and ABC is caused by interaction of layers that are  $2c$  apart and therefore it is very small, of around  $3\mu\text{eV/atom}$ .

The explanation to AB:ABC ratio observed, of about

80:14 ([60]), could be found by adding to already existing isotropic attractive term of vdW potential a small anisotropic contribution to equations like these of KC or Lebedeva. Since interplane binding is caused by strongly anisotropic interaction between  $\pi$  orbitals one would expect that not only repulsive but also attractive component of that interaction is anisotropic.

#### Raman shifts in LBM and shear modes ( $C_{33}$ and $C_{44}$ elastic constants)

Early neutron scattering measurements confirmed the existence of the low-frequency acoustic mode in bulk pyrolytic graphite [69], that is longitudinal waves in the direction of the hexagonal axis, at  $3.84 \pm 0.06\text{ THz}$ . The transverse waves (in shear mode) were less pronounced, at  $1.3 \pm 0.3\text{ THz}$ . Based on these data elas-

tic constants have been deduced,  $C_{33} = 39 \pm 4 \text{ GPa}$  (for direction perpendicular to graphite planes; LBM), and  $C_{44} = 4.2 \pm 2 \text{ GPa}$  (shear mode parallel to planes). These values correspond to Raman shift energies of 130 and 43  $\text{cm}^{-1}$ , in agreement with several DFT calculations [70]. The experimental evidence of the longitudinal mode was reported in ultrafast laser pump-probe spectroscopy [71] on FLG, at  $\sim 120 \text{ cm}^{-1}$ , demonstrating also the presence there of the phonon and electron coupling through the Breit-Wigner-Fano resonance, as at more pronounced G-mode [72].

Position of peaks in both LBM and shear modes is a geometrical effect and depends strongly on the number of layers in FLG. Moreover, unique multippeak features are observed, characteristic for the number of layers investigated. Their frequencies in case of LBM [73] mode are described well using a simple linear-chain model based on nearest-neighbor couplings between the layers [74]:

$$\omega_N(n) = \omega_0 \sin[(N - n)\pi/2N], \quad (13)$$

where  $\omega_0$  is the frequency of the bulk mode,  $N$  is the number of layers in FLG and  $n$  enumerates observed Raman frequencies. It follows from measurements that in the limit of large number of layers the bulk LBM Raman peak should have value of  $264.5 \text{ cm}^{-1}$  [73].

For shear mode, the nature of interactions between planes, their collective behaviour, leads to quantitatively similar dependence of Raman frequencies on the number of layers in FLG as in the case of LBM mode: the frequency in the bulk is  $\sqrt{2}$  times larger than for bilayer graphene [75], [76]. Its frequency depends on energy difference between AB and AA stacking. For that reason it is sensitive to the choice of inter-plane interaction potential.

In Fig. 6 we show how the potential energy changes when a graphene plane lying in a distance of  $3.35 \text{ \AA}$  over another graphene plane moves away from AB position for  $1.42 \text{ \AA}$ , towards AA stacking. These calculations were made in LAMMPS, assuming LJ potential with  $\sigma = 3.4322 \text{ \AA}$  and  $\epsilon = 2.4 \text{ meV}$ . We find that the energy difference between planes in AA and AB positions is of around  $1 \text{ meV/atom}$ , only, at  $P = 0 \text{ GPa}$ .

By having the curvature of parabolic potential wells at low-values of departure from optimal position of both layers (in AB stacking; we used data for  $x$  less than  $0.05 \text{ \AA}$ ) we are able to compute Raman frequencies in shear mode in a broad range of pressure. The curvature  $k$  of parabolic fit of data in Figure 6,  $E_p(x) - E_{AB} = k/2 \cdot x^2$ , with equation  $R[\text{cm}^{-1}] = \sqrt{2} \cdot \sqrt{k} \cdot 703$ , where  $k$  is in  $\text{eV/\AA}^2$  and  $R$  is the Raman shift. The  $\sqrt{2}$  factor is to account that the bulk potential acting on a plane is twice as large as potential for single plane on the surface of sample.

Results on Raman shift are shown in Fig. 7, where a comparison is made of the data obtained by using LJ,

Lebedeva and KC potential models (for KC with two sets of parameters), as listed in Tables III, IV. The data in Fig. 7 are compared with experimental results of Hanfland et al. [59]. It is evident that LJ potential can not describe well measured values of Raman shift while both, KC and Lebedeva models, allow to achieve an acceptable fit to real data. We observe also that LJ frequency shift at  $P = 0 \text{ GPa}$  is about twice too low to explain the Raman shift observed in experiment. This means that the energy difference between AA and AB arrangement of planes must be around  $5 \text{ meV}$  per atom at  $P = 0 \text{ GPa}$ , which is significantly smaller than reported in some DFT calculations [31], [48].

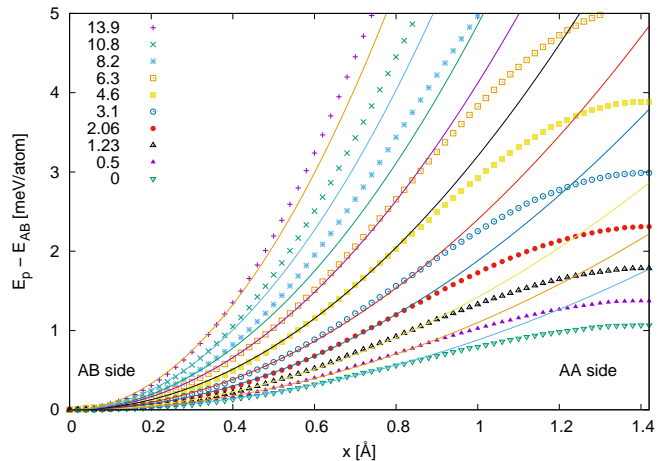


FIG. 6: Datapoints show change in potential energy of a plane that is moved from AB position over another large plane, for distance equal to  $a=1.42 \text{ \AA}$ , which results in AA position, under several values of pressure [GPa], as listed in the legend. The classical 12-6 Lennard-Jones potential was used in modelling, with  $\sigma = 3.4322 \text{ \AA}$  and  $\epsilon = 2.4 \text{ meV}$ . Solid lines show a tentative fit of parabolic dependencies.

For LBM mode results on the Raman shift are known at  $P = 0 \text{ GPa}$ , only, and our model predicts that value accurately [73]. In this case there is no need to use LAMMPS in computation. The scheme described in this section offers an alternate and convenient way of numerical computing frequency of oscillations from potential energy curvature by starting with Eq. 8. We need to use also the data available in Fig. 5 and find out from there how planes' spacing  $c$  changes with pressure. We insert  $c$  values into Eq. 8 and numerically find out the second derivative  $d^2 E_{AB}(z)/dz^2$ , which gives us curvature of potential minimum and, next, frequencies of Raman shift, as a function of pressure.

Figure 8 shows pressure dependence of Raman shift in LBM mode computed for LJ, KC and Lebedeva models, by using this method. If similar experimental data were available we could have an additional indication on which of considered models of vdW interactions fits best to reality.

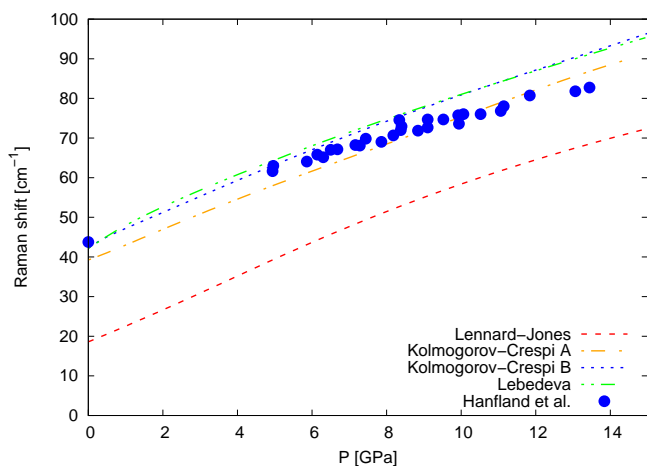


FIG. 7: Raman shift energy as a function of pressure, for bulk shear mode. The lines are computed from curvature  $k$  of parabolic fit of data in Figure 6. Blue circles are experimental data of Hanfland et al. [59].

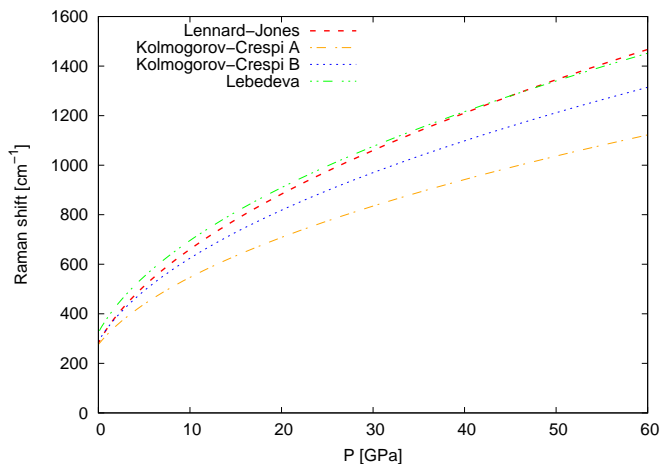


FIG. 8: Predicted pressure dependence of Raman shift for LBM mode of bulk graphite.

## SUMMARY AND CONCLUSIONS.

Interlayer interaction modeling in graphenites based on phenomenological van der Waals potentials (Lennard-Jones, Kolmogorov-Crespi and Lebedeva's) was performed. Results have been compared self-consistently with ab-initio calculations and experimental data on compressibility and Raman shifts in LBM and shear modes under pressure, favoring strongly anisotropic Kolmogorov-Crespi model. Computation was done by using molecular dynamics package LAMMPS and a proposed convenient, extendable scheme of computation suitable for fast numerical modeling of several physical quantities. The method is useful for studying other 2-dimensional homo- and heterostructures with van der Waals type interaction between layers. It is argued that

the value of the known Raman shift in shear mode is consistent with the difference in energy between AA and AB stacking of around 5 meV per atom. The models do not provide explanation for the reported low content of ABC stacking in natural graphite.

- 
- [1] A. K. Geim and I. V. Grigorieva. Van der waals heterostructures. *Nature*, 499:419–425, 2013. doi: 10.1038/nature12385. URL <http://dx.doi.org/10.1038/nature12385>.
  - [2] Nam B. Le, Tran Doan Huan, and Lilia M. Woods. Interlayer interactions in van der waals heterostructures: Electron and phonon properties. *ACS Appl. Mater. Interfaces*, 9(9):6286–6292, 2016. doi: 10.1021/acsami.6b00285. URL <http://dx.doi.org/10.1021/acsami.6b00285>.
  - [3] M M van Wijk, A Schuring, M I Katsnelson, and A Fasolino. Relaxation of moiré patterns for slightly misaligned lattices: graphene on graphite. *2D Materials*, 2(3):034010, 2015. doi: 10.1088/2053-1583/2/3/034010. URL <http://doi.org/10.1088/2053-1583/2/3/034010>.
  - [4] M M van Wijk, A Schuring, M I Katsnelson, and A Fasolino. Moiré patterns as a probe of interplanar interactions for graphene on h-bn. *Phys. Rev. Lett.*, 113:135504, 2014. doi: 10.1103/PhysRevLett.113.135504. URL <http://doi.org/10.1103/PhysRevLett.113.135504>.
  - [5] Yuan Cao, Valla Fatemi, Shiang Fang, Kenji Watanabe, Takashi Taniguchi, Efthimos Kaxiras, and Pablo Jarillo-Herrero. Unconventional superconductivity in magic-angle graphene superlattices. *Nature*, 2018. doi: <http://dx.doi.org/10.1038/nature26160>. URL <http://dx.doi.org/10.1038/nature26160>.
  - [6] Han Peng, Niels B. M. Schröter, Jianbo Yin, Huan Wang, Ting-Fung Chung, Haifeng Yang, Sandy Ekhana, Zhongkai Liu, Juan Jiang, Lexian Yang, Teng Zhang, Heng Ni Cheng Chen, Alexey Barinov, Yong P. Chen, Zhongfan Liu, Hailin Peng, and Yulin Chen. Substrate doping effect and unusually large angle van hove singularity evolution in twisted bi- and multilayer graphene. *Adv. Mater.*, page 1606741, 2017. doi: 10.1002/adma.201606741. URL <http://doi.org/10.1002/adma.201606741>.
  - [7] Giacomo Argentero, Andreas Mittelberger, Mohammad Reza Ahmadpour Monazam, Yang Cao, Timothy J. Penneycook, Clemens Mangler, Christian Kramberger, Jani Kotakoski, A. K. Geim, , and Jannik C. Meyer. Unraveling the 3d atomic structure of a suspended graphene/hbn van der waals heterostructure. *Nano Lett.*, 17:1409–1406, 2017. doi: <http://doi.org/10.1021/acs.nanolett.6b04360>. URL <http://doi.org/10.1021/acs.nanolett.6b04360>.
  - [8] Shisheng Lin, Yanghua Lu, Juan Xu, Sirui Feng, and Jianfeng Li. High performance graphene/semiconductor van der waals heterostructure optoelectronic devices. *Nano Energy*, 40:122–148, 2017. doi: 10.1016/j.nanoen.2017.07.036. URL <https://doi.org/10.1016/j.nanoen.2017.07.036>.
  - [9] Grigory Skoblin, Jie Sun, and August Yurgens. Graphene bolometer with thermoelectric readout and capacitive coupling to an antenna. *Appl. Phys. Lett.*, 112:063501,

2018. doi: <http://doi.org/10.1063/1.5009629>. URL <https://doi.org/10.1063/1.5009629>.
- [10] Xia Wei, Fa-Guang Yan, Chao Shen, Quan-Shan Lv, and Kai-You Wang. Photodetectors based on junctions of two-dimensional transition metal dichalcogenides. *Chinese Phys. B* 26, 26 (3):038504, 2017. doi: 10.1088/1674-1056/26/3/038504. URL <https://doi.org/10.1088/1674-1056/26/3/038504>.
- [11] Mu Congpu, Xiang Jianyong, and Liu Zhongyuan. Photodetectors based on sensitized two-dimensional transition metal dichalcogenides—a review. *Journal of Materials Research*, 32(22):4115–4131, 2017. doi: 10.1557/jmr.2017.402.
- [12] M Houssa, A Dimoulas, and A Molle. Silicene: a review of recent experimental and theoretical investigations. *Journal of Physics: Condensed Matter*, 27(25):253002, 2015. URL <http://stacks.iop.org/0953-8984/27/i=25/a=253002>.
- [13] D. G. Kvashnin and L. A. Chernozatonskii. Electronic and transport properties of heterophase compounds based on mos2. *Jetp Lett.*, 105:250, 2017. doi: 10.1134/S0021364017040117. URL <http://doi.org/10.1134/S0021364017040117>.
- [14] M. Luo, Y. H. Shen, and T. L. Yin. Structural, electronic, and magnetic properties of transition metal doped res2 monolayer. *Jetp Lett.*, 105: 255, 2017. doi: 10.1134/S0021364017040038. URL <http://doi.org/10.1134/S0021364017040038>.
- [15] Matthew Z. Bellus, Ming Li, Samuel D. Lane, Frank Ceballos, Qiannan Cui, Xiao Cheng Zeng, and Hui Zhao. Type-i van der waals heterostructure formed by mos2 and res2 monolayers. *Nanoscale Horiz.*, 2: 31–36, 2017. doi: 10.1039/C6NH00144K. URL <http://doi.org/10.1039/C6NH00144K>.
- [16] Faguang Yan, Lixia Zhao, Amalia Patané, PingAn Hu, Xia Wei, Wengang Luo, Dong Zhang, Quanshan Lv, Qi Feng, Chao Shen, Kai Chang, Laurence Eaves, and Kaiyou Wang. Fast multicolor photodetectors based on graphene-contacted p-gase/n-inse van der waals heterostructures. *Nanotechnology*, 28(7):27LT01, 2017. doi: <http://doi.org/10.1088/1361-6528/aa749e>. URL <http://stacks.iop.org/0957-4484/28/i=27/a=27LT01>.
- [17] M. Luo, H. H. Yin, and J. H. Chu. Magnetic properties of a na-doped ws2 monolayer in the presence of an isotropic strain. *JETP Letters*, 6(10):672–676, 2017. doi: <http://doi.org/10.1134/S0021364017220039>. URL <http://doi.org/10.1134/S0021364017220039>.
- [18] Oriol Lopez Sanchez, Dmitry Ovchinnikov, Shikhar Misra, Adrien Allain, and Andras Kis. Valley polarization by spin injection in a light-emitting van der waals heterojunction. *Nano Lett.*, 16:5792–5797, 2016. doi: <http://doi.org/10.1021/acs.nanolett.6b02527>.
- [19] Mallikarjuna Gurram, Siddhartha Omar, and Bart J. van Wees. Bias induced up to 100ferromagnet/bilayer-hbn/graphene/hbn heterostructures. *Nature Communications*, 8:248, 2017. doi: <http://doi.org/10.1038/s41467-017-00317-w>.
- [20] Jaewoo Shim, Seo-Hyeon Jo, Minwoo Kim, Young Jae Song, Jeehwan Kim, and Jin-Hong Park. Light-triggered ternary device and inverter based on heterojunction of van der waals materials. *ACS Nano*, 11(6):6319–6327, 2017. doi: <http://doi.org/10.1021/acsnano.7b02635>.
- [21] Wei Li, Xinlian Wang, and Xianqi Dai. Tunable schottky contacts in the antimonene/graphene van der waals heterostructures. *Solid State Communications*, 254: 37–41, 2017. doi: 10.1016/j.ssc.2017.02.008. URL <https://doi.org/10.1016/j.ssc.2017.02.008>.
- [22] K. H. Michel, D. Çakır, C. Sevik, and F. M. Peeters. Piezoelectricity in two-dimensional materials: Comparative study between lattice dynamics and ab initio calculations. *Phys. Rev. B*, 95:125415, 2017. doi: <https://doi.org/10.1103/PhysRevB.95.125415>.
- [23] Shigeki Kawai, Adam S. Foster, Torbjörn Björkman, Sylwia Nowakowska, Jonas Björk, Filippo Federici Canova, Lutz H. Gade, Thomas A. Jung, and Ernst Meyer. Van der waals interactions and the limits of isolated atom models at interfaces. *Nature Communications*, 7:11559, 2016. doi: 10.1038/ncomms11559. URL <http://dx.doi.org/10.1038/ncomms11559>.
- [24] A.V. Rozhkov, A.O. Sboychakov, A.L. Rakhmanov, and Franco Nori. Electronic properties of graphene-based bilayer systems. *Physics Reports*, 648:1–104, 2016. doi: 10.1016/j.physrep.2016.07.003. URL <http://dx.doi.org/10.1016/j.physrep.2016.07.003>.
- [25] L. A. Girifalco and Miroslav Hodak. Van der waals binding energies in graphitic structures. *Phys. Rev. B*, 65: 125404, 2002. doi: 10.1103/PhysRevB.65.125404. URL <http://doi.org/10.1103/PhysRevB.65.125404>.
- [26] J.-C. Charlier, X. Gonze, and J.-P. Michenaud. Graphite interplanar bonding: Electronic delocalization and van der waals interaction. *Europhysics Letters*, 28:403, 1994. URL <http://stacks.iop.org/0295-5075/28/i=6/a=005>.
- [27] S. B. Trickey, F. Müller-Plathe, G. H. F. Diercksen, and J. C. Boettger. Interplanar binding and lattice relaxation in a graphite dilayer. *Physical Review B*, 46:4460, 1992. doi: 10.1103/PhysRevB.45.4460. URL <http://doi.org/10.1103/PhysRevB.45.4460>.
- [28] H. Rydberg, M. Dion, N. Jacobson, E. Schröder, P. Hyldgaard, S. I. Simak, D. C. Langreth, and B. I. Lundqvist. Van der waals density functional for layered structures. *Physical Review Letters*, 91:126402, 2003. doi: 10.1103/PhysRevLett.91.126402. URL <https://doi.org/10.1103/PhysRevLett.91.126402>.
- [29] D. P. DiVincenzo, E. J. Mele, and N. A. W. Holzwarth. Density-functional study of interplanar binding in graphite. *Physical Review B*, 27: 2458, 1983. doi: 10.1103/PhysRevB.27.2458. URL <https://doi.org/10.1103/PhysRevB.27.2458>.
- [30] Matthias C. Schabel and José Luís Martins. Energetics of interplanar binding in graphite. *Physical Review B*, 46:7185, 1992. doi: 10.1103/PhysRevB.46.7185. URL <https://doi.org/10.1103/PhysRevB.46.7185>.
- [31] E. Mostaani, N. D. Drummond, and V. I. Fal’ko. Quantum monte carlo calculation of the binding energy of bilayer graphene. *Phys. Rev. Lett.*, 115:115501, 2015. doi: 10.1103/PhysRevLett.115.115501. URL <https://doi.org/10.1103/PhysRevLett.115.115501>.
- [32] M. Birowska, K. Milowska, and J.A. Majewski. Van der waals density functionals for graphene layers and graphite. *Acta Physica Polonica A*, 120(5):845, 2011. URL <http://przyrbwn.icm.edu.pl/APP/PDF/116/a116z520.pdf>.
- [33] S. D. Chakarova-Kack, E. Schroder, B. I. Lundqvist, and D. C. Langreth. Application of van der waals density functional to an extended system: Adsorption of benzene and naphthalene on graphite. *Phys. Rev. Lett.*, 96:146107,

2006. doi: 10.1103/PhysRevLett.96.146107. URL <http://doi.org/10.1103/PhysRevLett.96.146107>.
- [34] Jian Ping Lu, X.-P. Li, and Richard M. Martin. Ground state and phase transitions in solid c60. *Phys. Rev. Lett.*, 68:1551, 1992. doi: 10.1103/PhysRevLett.68.1551. URL <https://doi.org/10.1103/PhysRevLett.68.1551>.
- [35] L.Y. Jiang, Y. Huang, H. Jiang, G. Ravichandran, H. Gao and K.C. Hwang, and B. Liu. A cohesive law for carbon nanotube/polymer interfaces based on the van der waals force. *Journal of the Mechanics and Physics of Solids*, 54:2436–2452, 2006. doi: 10.1016/j.jmps.2006.04.009. URL <http://doi.org/10.1016/j.jmps.2006.04.009>.
- [36] X.Q. He, S. Kitipornchai, and K.M. Liew. Buckling analysis of multi-walled carbon nanotubes: a continuum model accounting for van der waals interaction. *Journal of the Mechanics and Physics of Solids*, 53:303–326, 2005. doi: 10.1016/j.jmps.2004.08.003. URL <http://doi.org/10.1016/j.jmps.2004.08.003>.
- [37] S. Kitipornchai, X. Q. He, and K. M. Liew. Continuum model for the vibration of multilayered graphene sheets. *Phys. Rev. B*, 72:075443, 2005. doi: 10.1103/PhysRevB.72.075443. URL <http://doi.org/10.1103/PhysRevB.72.075443>.
- [38] H. Tan, L.Y. Jiang, Y. Huang, B. Liu, and K.C. Hwang. The effect of van der waals-based interface cohesive law on carbon nanotube-reinforced composite materials. *Composites Science and Technology*, 67(14):2941–2946, 2007. doi: 10.1016/j.compscitech.2007.05.016. URL <https://doi.org/10.1016/j.compscitech.2007.05.016>.
- [39] Gustav Mie. Zur kinetischen theorie der einatomigen körper. *Ann Phys*, 316:657, 1903. doi: 10.1002/andp.19033160802. URL <http://dx.doi.org/10.1002/andp.19033160802>.
- [40] C. Avendano, T. Lafitte, A. Galindo, C. S. Adjiman, G. Jackson, and E. Muller. Soft- $\gamma$  force field for the simulation of molecular fluids. 1. a single-site coarse grained model of carbon dioxide. *J Phys Chem B*, 115:11154, 2011. doi: 10.1021/jp204908. URL <http://dx.doi.org/10.1021/jp204908>.
- [41] Aleksey N. Kolmogorov and Vincent H. Crespi. Smoothest bearings: interlayer sliding in multiwalled carbon nanotubes. *Phys. Rev. Lett.*, 85(22):4727–4730, 2000. doi: 10.1103/PhysRevLett.85.4727. URL <http://doi.org/10.1103/PhysRevLett.85.4727>.
- [42] Aleksey N. Kolmogorov and Vincent H. Crespi. Registry-dependent interlayer potential for graphitic systems. *Physical Review B*, 71(23):235415, 2005. doi: 10.1103/PhysRevB.71.235415. URL <https://doi.org/10.1103/PhysRevB.71.235415>.
- [43] S. Plimpton. Fast parallel algorithms for short-range molecular dynamics. *J Comp Phys*, 117, 1-19 (1995), 117:1–19, 1995. URL <http://lammps.sandia.gov>.
- [44] M. M. van Wijk, A. Schuring, M. I. Katsnelson, and A. Fasolino. Moiré patterns as a probe of interplanar interactions for graphene on h-bn. *Phys. Rev. Lett.*, 113:135504, 2014. doi: 10.1103/PhysRevLett.113.135504. URL <http://dx.doi.org/10.1103/PhysRevLett.113.135504>.
- [45] Annelot Schuring. Moiré patterns in graphene in hexagonal substrates. *Radboud University Nijmegen*, Master Thesis, 2014.
- [46] Tuck Wah Ng, Chun Yat Lau, Esteban Bernados-Chamagne, Jefferson Zhe Liu, John Sheridan, and Ne Tan. Graphite flake self-retraction response based on potential seeking. *Nanoscale Res Lett.*, 7(1):185, 2012. doi: 10.1103/PhysRevB.93.235414. URL <http://doi.org/10.1103/PhysRevB.93.235414>.
- [47] Roberto Guerra, Ugo Tartaglino, Andrea Vanossi, and Erio Tosatti. Ballistic nanofriction. *Nature Materials*, 9:634–637, 2010. doi: 10.1038/nmat2798. URL <http://doi.org/10.1038/nmat2798>.
- [48] Irina V. Lebedeva, Andrey A. Knizhnik, Andrey M. Popov, Yurii E. Lozovik, and Boris V. Potapkin. Modeling of graphene-based nems. *Physica E*, 44(6):949–954, 2012. doi: 10.1016/j.physe.2011.07.018. URL <https://doi.org/10.1016/j.physe.2011.07.018>.
- [49] Irina V. Lebedeva, Andrey A. Knizhnik, Andrey M. Popov, Yurii E. Lozovik, and Boris V. Potapkin. Molecular dynamics simulation of the self-retracting motion of a graphene flake. *Phys. Rev. B*, 84:245437, 2011. doi: 10.1103/PhysRevB.84.245437. URL <https://doi.org/10.1103/PhysRevB.84.245437>.
- [50] Jin-Wu Jiang. Registry effect on the thermal conductivity of few-layer graphene. *Journal of Applied Physics*, 116:164313, 2014. doi: 10.1063/1.4900526. URL <http://dx.doi.org/10.1063/1.4900526>.
- [51] V. Baskin and L. Meyer. Lattice constants of graphite at low temperatures. *Phys. Rev. B*, 100(2):544, 1955. doi: 10.1103/PhysRevB.100.544. URL <http://doi.org/10.1103/PhysRevB.100.544>.
- [52] C. H. Kiang, M. Endo, P. M. Ajayan, G. Dresselhaus, and M. S. Dresselhaus. Size effects in carbon nanotubes. *Phys. Rev. Lett.*, 81(9):1869, 1998. doi: 10.1103/PhysRevLett.81.1869. URL <http://doi.org/10.1103/PhysRevLett.81.1869>.
- [53] P. Trucano and R. Chen. Structure of graphite by neutron diffraction. *Nature*, 258:136, 1975.
- [54] Wei Gao and Rui Huang. Effect of surface roughness on adhesion of graphene membranes. *J. Phys. D: Appl. Phys.*, 44:452001, 2011. URL <http://stacks.iop.org/0022-3727/44/i=45/a=452001>.
- [55] Yuejian Wang, Joseph E. Panzik, Boris Kiefer, and Kanani K. M. Lee. Crystal structure of graphite under room-temperature compression and decompression. *Scientific Reports*, 2:520, 2012. doi: 10.1038/srep00520. URL <http://doi.org/10.1038/srep00520>.
- [56] R. W. Lynch and H. G. Drickamer. Effect of high pressure on the lattice parameters of diamond, graphite, and hexagonal boron nitride. *The Journal of Chemical Physics*, 44:181, 1966. doi: <http://doi.org/10.1063/1.1726442>. URL <http://doi.org/10.1063/1.1726442>.
- [57] You Xiang Zhao and Ian L. Spain. X-ray diffraction data for graphite to 20 gpa. *Phys. Rev. B*, 40(2):993, 1989. doi: 10.1103/PhysRevB.40.993. URL <http://doi.org/10.1103/PhysRevB.40.993>.
- [58] S.M. Clark, Ki-Joon Jeon, Jing-Yin Chen, and Choong-Shik Yoo. Few-layer graphene under high pressure: Raman and x-ray diffraction studies. *Solid State Communications*, 154:15–18, 2013. doi: 10.1016/j.ssc.2012.10.002. URL <http://doi.org/10.1016/j.ssc.2012.10.002>.
- [59] M. Hanfland, H. Beister, and K. Syassen. Graphite under pressure: Equation of state and first-order raman modes. *Phys Rev B*, 39:12598, 1989. doi: 10.1103/PhysRevB.39.12598. URL <http://doi.org/10.1103/PhysRevB.39.12598>.
- [60] H. Lipson and A.R. Stokes. The structure of graphite. *Proc. Roy. Soc. A*, 181:101–105, 1942.

- [61] Jae-Kap Lee, Seung-Cheol Lee, Jae-Pyoung Ahn, Soo-Chul Kim, John I. B. Wilson, and Phillip John. The growth of aa graphite on (111) diamond. *J. Chem. Phys.*, 129:234709, 2008. doi: 10.1063/1.2975333. URL <http://dx.doi.org/10.1063/1.2975333>.
- [62] J. R. Dahn, Rosamaria Fong, and M. J. Spoon. Suppression of staging in lithium-intercalated carbon by disorder in the host. *Phys. Rev. B*, 42:6424, 1990. doi: 10.1103/PhysRevB.42.6424. URL <https://doi.org/10.1103/PhysRevB.42.6424>.
- [63] Wataru Norimatsu and Michiko Kusunoki. Selective formation of abc-stacked graphene layers on sic(0001). *Phys. Rev. B*, 81:161410, 2010. doi: 10.1103/PhysRevB.81.161410. URL <http://doi.org/10.1103/PhysRevB.81.161410>.
- [64] J.-C. Charlier, X. Gonze, and J.-P. Michenaud. First-principles study of the electronic properties of graphite. *Phys. Rev. B*, 43:4579, 1991. doi: 10.1103/PhysRevB.43.4579. URL <http://doi.org/10.1103/PhysRevB.43.4579>.
- [65] Kazunari Yoshizawa, Takashi Kato, and Tokio Yamabe. Interlayer interactions in two-dimensional systems: Second-order effects causing abab stacking of layers in graphite. *J. Chem. Phys.*, 105(5):2099, 1996. doi: <http://dx.doi.org/10.1063/1.472076>. URL <http://dx.doi.org/10.1063/1.472076>.
- [66] J. C. Charlier, X. Gonze, and J. P. Michenaud. First-principles study of the stacking effect on the electronic properties of graphite(s). *Carbon*, 32 (2):289–299, 1994. doi: [https://doi.org/10.1016/0008-6223\(94\)90192-9](https://doi.org/10.1016/0008-6223(94)90192-9). URL [https://doi.org/10.1016/0008-6223\(94\)90192-9](https://doi.org/10.1016/0008-6223(94)90192-9).
- [67] W. Gao and A. Tkatchenko. Sliding mechanisms in multilayered hexagonal boron nitride and graphene: The effects of directionality, thickness, and sliding constraints. *Phys. Rev. Lett.*, 114:096101, 2015. doi: 10.1103/PhysRevLett.114.096101. URL <https://doi.org/10.1103/PhysRevLett.114.096101>.
- [68] Wang Tao, Guo Qing, Liu Yan, and Sheng Kuang. A comparative investigation of an ab- and aa-stacked bilayer graphene sheet under an applied electric field: A density functional theory study. *Chin. Phys. B*, 21:067301, 2012. doi: 10.1088/1674-1056/21/6/067301. URL <http://doi.org/10.1088/1674-1056/21/6/067301>.
- [69] G. Dolling and B. N. Brockhouse. Lattice vibrations in pyrolytic graphite. *Phys. Rev.*, 128:1120, 1962. doi: 10.1103/PhysRev.128.1120. URL <https://doi.org/10.1103/PhysRev.128.1120>.
- [70] Alexander V. Lebedev, Irina V. Lebedeva, Andrey M. Popov, and Andrey A. Knizhnik. Stacking in incommensurate graphene/hexagonal-boron-nitride heterostructures based on ab initio study of interlayer interaction. *Phys. Rev. B*, 96:085432, 2017. doi: 10.1103/PhysRevB.96.085432. URL <https://doi.org/10.1103/PhysRevB.96.085432>.
- [71] Jingzhi Shang, Chunxiao Cong, Jun Zhang, Qihua Xiong, Gagik G. Gurzadyan, and Ting Yu. Observation of low-wavenumber out-of-plane optical phonon in few-layer graphene. *J Raman Spec*, 40:70–74, 2013. doi: 10.1002/jrs.4141. URL <http://doi.org/10.1002/jrs.4141>.
- [72] J. M. Baranowski, M. Mozdzonek, P. Dabrowski, K. Grodecki, P. Osewski, W. Kozlowski, M. Kopciszynski, M. Jalochowski, and W. Strupinski. Observation of electron-phonon couplings and fano resonances in epitaxial bilayer graphene. *Graphene*, 2:115–120, 2013. doi: <http://dx.doi.org/10.4236/graphene.2013.24017>. URL <http://dx.doi.org/10.4236/graphene.2013.24017>.
- [73] Chun Hung Lui and Tony F. Heinz. Measurement of layer breathing mode vibrations in few-layer graphene. *Phys. Rev. B*, 87:121404, 2013. doi: 10.1103/PhysRevB.87.121404. URL <http://doi.org/10.1103/PhysRevB.87.121404>.
- [74] Steven T. Thornton and Jerry B. Marion. Classical dynamics of particles and systems. *Fifth Edition*, Brooks Cole, Pacific Grove, CA, 2003.
- [75] P. H. Tan, W. P. Han, 1 Z. H. Wu W. J. Zhao, K. Chang, H. Wang, Y. F. Wang, N. Bonini, N. Marzari, G. Savini, A. Lombardo, and A. C. Ferrari. The shear mode of multilayer graphene. *Nat. Mater.*, 11:294–300, 2012. doi: <http://doi.org/10.1038/nmat3245>.
- [76] Chunxiao Cong and Ting Yu. Enhanced ultra-low-frequency interlayer shear modes in folded graphene layers. *Nature Communications*, 5:4709, 2014. doi: 10.1038/ncomms5709. URL <http://doi.org/10.1038/ncomms5709>.
- [77] LAMMPS implementation of equation of Lebedeva et al. is available from the corresponding author.